Journal of the Chinese Society of Mechanical Engineers, Vol.47, No.2, pp 195~202 (2026)

Residual Mechanical Properties of Cold-Worked Austenitic Stainless-Steel Reinforcing Rebar After Exposure to Elevated Temperatures: A Non-linear Analysis

Haitham Abdallah Khamis AL Adawani*, Tuan Zaharinie Tuan Zahari*,** and Muhammad Khairi Faiz bin Ahmad Hairuddin*,**

Keywords : Stainless steel, Residual mechanical properties, EN1.4401 Austenitic stainless steel reinforcing bars, Proof strength, Ultimate tensile strength.

ABSTRACT

This study focuses on the finite element analysis of the residual mechanical properties of 316 EN 1.4401 cold-worked austenitic stainless steel reinforcing bars, compared to experimental results. The study assessed the influence of user-defined material properties on an isotropic elasticity model and a multilinear isotropic hardening model, evaluated under different conditions to validate against experimental observations. This study demonstrated a strong correlation between experimental results and numerical simulations, showing only slight differences in the residual mechanical response across various cooling methods. The investigation revealed a high correlation between total maximum strain (mm/mm) and user-defined (the total elastic and plastic strain). The variation in ultimate tensile strength (f_u) between the experimental and numerical results is less than 2% except for one case which involving slow cooling inside furnace at 500°C (2.5%). Likewise, the difference in 0.2% proof strength ($f_{0.2p}$) is below 2.5%, except for three cases involving rapid water cooling at 500°C (3.2%) and intermediate air cooling at 500°C (3.3%) and 500°C (3.8%) respectively. Therefore, the numerical methods can enhance the precision of experimental results for assessing structural characteristics.

Paper Received December, 2024. Revised March, 2025. Accepted May, 2025. Author for Correspondence:Tuan Zaharinie Tuan Zahari.

* *Department of Mechanical Engineering, Universiti Malaya, 50603 Kuala Lumpur, Malaysia.*

** *Centre of Advanced Manufacturing and Material Processing, Universiti Malaya, 50603 Kuala Lumpur, Malaysia.*

INTRODUCTION

Over the past century, the durability and aesthetic qualities of stainless steel have inspired architects and designers to utilize this material in a diverse array of both practical and imaginative applications. Apart from the minimum 10.5% chromium required for stainless steel's corrosion resistance, it may contain various other alloying elements, such as carbon, nickel, manganese, molybdenum, copper, silicon, sulfur, phosphorus, and nitrogen as defined by (Amanat, 2025). The incorporation of different alloying elements into stainless steels significantly improves their structure and properties in five essential areas: 1) Enhanced corrosion resistance, 2) Elevated strength at elevated temperatures, 3) Improved formability, 4) Increased ductility, and 5) Superior properties at high temperatures (Järvenpää et al., 2020). In addition, the incorporation of these alloying elements is essential for enhancing the performance and adaptability of stainless steel across various applications as clarified by (Sun et al., 2022).

The metallurgical composition of stainless steel is influenced by these alloying elements, resulting in the classification of stainless steels into five categories including austenitic, ferritic, austenitic–ferritic (duplex), martensitic, and precipitation hardening stainless steels as depicted in Figure 1(Shen & Chacón, 2019). The first three types exhibit extensive and varied applications within the construction sector, including building exteriors, facades, and pedestrian bridges. The last two categories are designated for specialized applications as explained by (Baddoo, 2013).

For instance, austenitic stainless steel contains 17 to 18% chromium and 8 to 11% nickel, characterized by a face-centered cubic atomic structure as defined by (Meza et al., 2024). Austenitic stainless steel (ASS) is available in a wide range of grades, with the predominant types being 316 EN 1.4401 and 304 EN 1.4301 as clarified by (Moore & Steels, 2010) and

it can be fabricated into a diverse array of forms, including sheets, plates, and bars (rebars), among others. Consequently, ASS reinforcing bars are commonly utilized in structural applications.

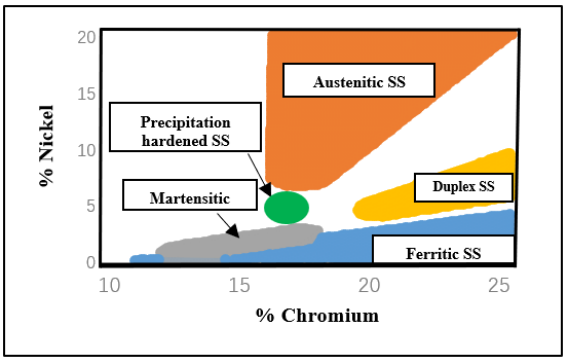

Figure 1. Types of stainless steel and their typical chemical compositions.

316 EN 1.4401 is often called marine-grade stainless steel due to its excellent performance in harsh seawater environments and it has molybdenum which makes it to be more resistant to pitting and crevice corrosion, higher tensile strength and maintaining strength and corrosion resistance at temperatures up to 925°C compared to other grades of austenitic stainless steel(Gudić et al., 2023). Therefore, it has been used in many areas such as in the river forth bridge in Scotland and in pedestrian bridge in Ortisei in Val Gardena, Italy. In addition, Hardman bridge Ottawa, built in 2014 with the use of grade EN 1.4401 austenitic stainless-steel reinforcement rebars.

Due to the excellent characteristics of EN 1.4401 ASS reinforced rebars, this has led to an increasing interest to utilize it across various study scenarios. For example, (Zapała et al., 2022), performed a static tensile test on EN 1.4401 using an instron 5566 device equipped with a heating furnace. The tests were conducted at temperatures of 200°C, 400°C, and 700°C. Each sample was held in the furnace for 15 minutes, and subjected to cooling in water and the result showed that as the testing temperature increased, both tensile and yield strengths significantly decreased, by around 60% and 38%, respectively. Elongation varied with temperature, showing higher ductility at 700°C than 200°C, though it was lower at 400°C. Furthermore, (Lv et al., 2022) performed tensile tests on EN 1.4401 utilizing an RDL-50 mechanical testing machine, maintaining a constant cross-head speed of 2 mm/min at temperatures of 20°C, 350°C, 450°C, 550°C, and 750°C. Specimens were maintained at the specified temperature for 15 minutes prior to testing to ensure a steady-state temperature and following by water cooling. This study found out that yield strength decreased gradually from 600 MPa at 20°C to lower values at 750°C and UTS exhibited a plateau between 350°C and 550°C, followed by a significant drop beyond 550°C. Moreover, (Rehman et al., 2022), examined the structural behavior of EN 1.4401, 1.4301 and 1.4436 austenitic stainless-steel reinforcing rebars before and after fire scenario, then compared with B500B conventional carbon steel. The materials were subjected to temperatures ranging from 100°C to 900°C for a duration of one hour while increasing at a speed of 10°C per minute. Subsequently, they underwent three different cooling conditions: fast cooling in water, gradual cooling in air, and furnace cooling as shown in Figure 2 which shows the stress-strain response for EN 1.4401 austenitic stainless steel reinforcement bars before and after being subjected to different temperatures and cooling modes. The study found that austenitic stainless-steel reinforcing rebars maintained their mechanical properties better than conventional carbon steel after exposure to high temperatures and subsequent cooling. The mechanical characteristics of the stainless-steel bars showed limited variation across repeated samples, and they retained their strength and ability to deform under different cooling conditions. Furthermore, metallurgical analysis revealed changes in the phase and grain structure of the stainless-steel bars.

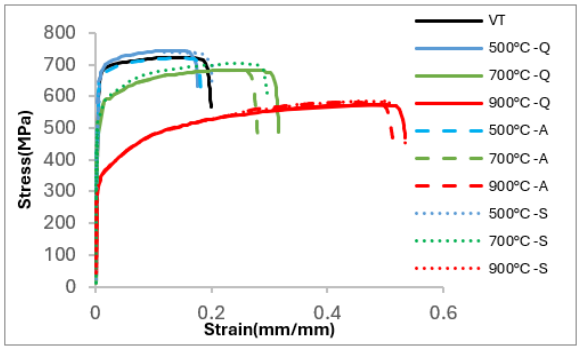

Figure 2. Stress-strain behavior of EN 1.4401 stainless steel reinforcement bars after being exposed to different temperature values (500°C, 700°C, and 900°C) using diverse cooling modes.

This study aims to investigate the residual mechanical performance of cold-worked EN 1.4401 austenitic stainless steel reinforcement bars through finite element analysis and validates the findings using experimental data. The conventional experimental methods for evaluating structural properties are complex and need extensive experimental effort. The accuracy of the results is uncertain, and validation of the findings can be accomplished via numerical methods. Thus, the numerical approaches used in this study will enhance the accuracy of the experimental results.

Experimental Testing Details

The experimental study, conducted by researchers and reported in the literature (Rehman et al., 2022) which examined the residual mechanical characteristics of cold-worked EN 1.4401 austenitic stainless-steel reinforcing bars after exposure to elevated temperatures. In this study, the mechanical tensile tests

were performed with an instron 5584 electromechanical testing frame with a load capacity of 150 kN. The samples were subjected to a preload of 10 kN before applying strain. The initial strain rate was 0.00007 s^{-1} until 1% strain was attained, after which the strain rate increased to 0.00025 s^{-1} until fracture occurred. Samples were heated to target temperatures ranging from 100 °C to 900 °C with the heating rate of 10 °C/min, maintained for 1 hour, and subsequently cooled using three methods as rapid cooling in water, gradual cooling in air, and furnace cooling, prior to tensile testing to evaluate residual mechanical properties. The chemical composition and diameter of the bars are shown in Table 1(EN, 1995).

Table 1. The chemical composition (%) of 316

Material bar and diameter	%C	%Mn	%Si	%S	%P	%Ni	%Cr	%Mo	%N	%Cu	%Ti	%V
Cold-worked316(⌀ 12 mm)	0.023	1.438	0.366	0.027	-	10.54	16.685	2.049	0.046	-	-	-

Table 2. Comparison between finite element analysis and experimental testing results

Samples	FE model		Experimental (Rehman et al., 2022)		
	Ultimate tensile strength (f_u) (MPa)	Proof strength ($f_{0.2p}$) (MPa)	Ultimate tensile strength (f_u) (MPa)	Proof strength ($f_{0.2p}$) (MPa)	%Difference in f_u & $f_{0.2p}$
Virgin	717.5	592.6	723.6	604.0	0.8% & 1.8%
500°C-Q	742.6	604.1	746.5	624.4	0.5 & 3.2%
700°C-Q	687.2	502.9	685.8	498.6	0.2% & 0.8%
900°C-Q	581.7	307.5	577.7	308.5	0.6% & 0.3%
500°C-A	718.3	627.7	722.4	606.9	0.5% & 3.3%
700°C-A	677.35	507.6	687.7	527.7	1.5% & 3.8%
900°C-A	593.8	306.7	586.2	309.1	1.2%&0.75%
500°C-S	742.6	646.6	741.7	630.0	2.5% & 0.1%
700°C-S	704	553.3	705.2	542.1	0.1% & 2%
900°C-S	593.9	295.2	589.2	297.4	0.7% & 0.7%

Numerical Finite Element Model

A computational investigation was carried out using the ANSYS Workbench platform to study the properties of an austenitic stainless steel reinforcement bar. A finite element model was generated to represent grade 316 (also referred to as Grade EN 1.4401), with specifications of 12 mm in diameter and 300 mm in length as illustrated in Figure 3. The samples were initially at ambient temperature and then subjected to a range of elevated temperatures from 500°C, 700°C to 900°C. Subsequently, three distinct cooling procedures were implemented: rapid quenching in water, gradual cooling within the furnace, and natural air cooling until reaching room temperature. These cooling methods were specifically designed to simulate the potential variations in cooling rates that could occur following a fire event, including scenarios of self-extinguishing firefighting efforts involving water.

The primary objective of this investigation was to assess the impact of these different cooling methods on the remaining material properties of this bar. This study also involved evaluating user-defined material properties for an isotropic elasticity model and a multilinear isotropic hardening model across different distinct scenarios, with the aim of validating the findings against experimental data.

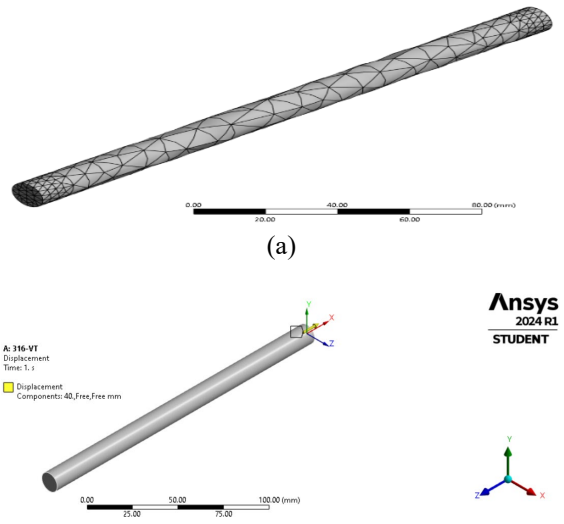

Figure 3. Finite element analysis was conducted on 316 austenitic stainless steel reinforcement bar, (a) including a coarse mesh model and (b) boundary conditions with one end fixed and the other end subjected to a 40 mm displacement load.

Due to the elastic and plastic behavior of austenitic stainless-steel bars, isotropic elasticity model which indicates the linear elastic behavior of austenitic stainless-steel bars. This model defines that the properties are same in all directions, with identical elastic modulus and Poisson's ratio. Table 2 contrasts the mechanical characteristics derived from the finite element analysis with the experimental findings presented in the literature (Rehman et al., 2022) . On the other hand, the multilinear isotropic hardening model for austenitic stainless-steel bar employs a piecewise linear function to represent the material's non-linear strain hardening behavior, effectively illustrating the stress-strain relationship until the onset of necking, while excluding the segment of the curve that exhibits a negative slope. This model assumes that the yield surface expands uniformly throughout plastic deformation, indicating that the material's strength increases consistently in all directions, while maintaining the shape of the yield surface.

The samples of 316 alloy were categorized based on their initial high-temperature exposure and the subsequent cooling method. The study investigated the 0.2% proof strength ($f_{0.2p}$) and ultimate tensile strength (f_u) of the material. These material properties were determined using experimental engineering stress-strain data, which was then converted to true stress-strain using standard equations.

$$\sigma_T = \sigma(1 + \varepsilon) \quad (1)$$

$$\varepsilon_T = \ln(1 + \varepsilon) \quad (2)$$

These are standard conversions between engineering and true stress and strain during uniaxial tensile testing, assuming volume constancy (no necking yet), where the true stress is denoted as σ_T and the engineering stress is denoted as σ, while the engineering strain is denoted as ε and the true strain is denoted as ε_T, so:

$$\sigma = \frac{\text{Load (Force)}}{\text{Original cross-sectional area } (A_0)} \quad (3)$$

$$\varepsilon = \frac{\text{Change in length } (\Delta L)}{\text{Original length } (L_0)} \quad (4)$$

Both of equations 3 & 4 are used to evaluate the extent of material elongation and the resistance it offers to applied force, under the assumption that the material maintains its shape without significant alteration. Whereas:

$$\sigma_T = \frac{\text{Load}}{\text{Instantaneous (current) cross-sectional area } (A)} \quad (5)$$

Therefore, equations 1, 2 & 5 are accurately representing the actual state of the material as it deforms, including plasticity, necking and reflecting what the material is truly experiencing and providing a more accurate representation of material behavior, particularly under large strains. especially when shape changes are large. Therefore, this is the reason behind converting engineering stress-strain into true stress-strain. However, engineering stress-strain data is simple but becomes physically wrong when large deformations happen (because area and strain evolution are nonlinear).

The true stress-strain data was then utilized to create the finite element model through the following summarized steps:

1- After converting engineering stress and strain into true stress and strain values, access the Engineering Data module, initiate the creation of a new material and name it as 316, and specify its elastic properties, including Young's modulus, which calculated in the experimental work (Rehman et al., 2022) and Poisson's ratio of 316 is 0.3. The 316 stainless steel reinforcement bar possesses a measured density of 7980 kg/m^3.

2- Select Multilinear Isotropic Hardening in the Plasticity section and enter the true plastic strain against true stress data.

3- Add Temperature-Dependent Data by clicking the "Temperature" column and inputting data for each temperature (e.g., 500 °C, 700 °C, 900 °C).

4- Assigning the material to geometry in the Model module by double-clicking the model cell and selecting the part/body under geometry, and then, set in the details pane, the material which is created.

5- Next, Setting the simulation parameters by
   a) A model Setup: using static structural, assigning geometry and refining the mesh.
   b) Assign the material: assigning a new material to the part.
   c) Use suitable elements: Use 3D solid which supports plasticity and large deformation.
   d) Analysis settings, enable large deflection and use automatic time stepping and ensure the load application is gradual to capture the material's plastic response accurately.ك The austenitic stainless-steel bar is fixed at one end, while the opposite end undergoes displacement loading at predefined sub steps as depicted in Figure 3(b). The displacement load was 40 mm across all temperature conditions for 316, except for 500 °C (fast cooling in water) where the displacement load increased to 45 mm. The finite element analysis utilizes an isotropic hardening model comprising multiple linear components and integrating the mesh elements into the finite element model is essential for achieving accurate results, as illustrated in Figure 3(a).

6- In reference to Figure 3(b), the coordinate system for the displacement is defined based on the displacement load value along the x-axis, with the y-axis and z-axis maintained at (0,0). As a result, the z-axis is determined by the Global x-axis. As previously indicated, the other bar end undergoes loading with displacement at designated sub-steps.

7- To achieve accurate results for the nonlinear properties of the bar, it is crucial to allow large deflection. Consequently, the subsequent parameters are derived: total deformation (mm), normal stress (MPa), equivalent stress (MPa), force reaction (N), EPTOX (mm/mm) which represents total plastic strain in the X-direction, EPELX (mm/mm) representing total elastic strain in the X-direction, EPPLX (mm/mm) indicating equivalent plastic strain in the X-direction, along with a user-defined result that is the sum of EPELX and EPPLX.

Ultimately, the ultimate tensile strength (f_u) (MPa) can be derived first from extracting the force reaction value (N) and total deformation value (mm) from FEA. Stress-strain data as shown as blue curve in Figure 4, this data can be obtained from equations 3 and 4 and then plotting it to find the ultimate tensile strength (f_u) (MPa) which is the maximum stress, which is 677.3531 MPa, which occurs at a strain of 0.042227. as shown as black dot in Figure 4, which depicts stress-strain curve with UTS and 0.2% proof strength for 700 °C in intermediate air cooling. Proof strength is the stress at which the material exhibits a permanent strain of 0.2% (i.e., 0.002 strain). It's used to define the yield point for materials without a clear yield plateau. It can be determined by the following:

a) First, creating the offset line by drawing a line parallel to the initial plastic portion of the stress-strain curve which in red dashed line in Figure 4, starting this line at a strain of 0.002 (which is 0.2% strain) and this line is called the 0.2% offset line.

b) Then, determining slope of plastic region (E) by choosing two points in the initial linear portion of the curve (usually where strain ≤ 0.005) and computing the slope by:

$$E = \frac{\Delta\sigma}{\Delta\varepsilon} \quad (6)$$

where Point 1: (0.004445, 507.60 MPa) and Point 2: (0.00889, 557.25 MPa)

$$E = \frac{557.25 - 507.60}{0.00889 - 0.004445} = \frac{49.65}{0.004445} \approx 11{,}169.83\text{MPa}$$

c) Next, defining 0.2% offset line equation, by line starts at (0.002,0), slope is E (from above) and the equation is

$$\sigma = E \cdot (\varepsilon - 0.002) \quad (7)$$

d) Finally, obtaining intersection with actual curve by going through the stress-strain data. For each strain value, calculate the offset stress using the above equation. Next to that, finding the first point where the actual stress is equal to or just exceeds the offset stress. That stress value is the 0.2% proof strength.

e) At strain = 0.004445, stress = 507.60 MPa. This is also where the offset line intersects the curve, so 0.2% Proof Strength = 507.60 MPa at shown is green dot in Figure 4.

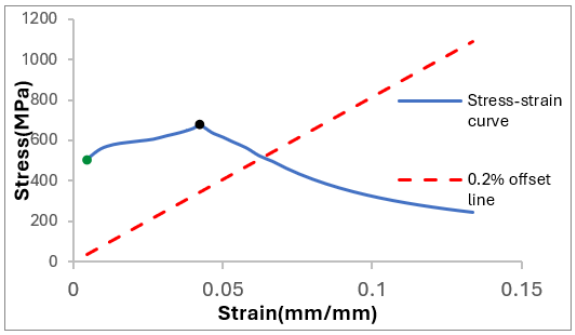

Figure 4. Stress-Strain Curve with UTS and 0.2% Proof Strength for 700 °C following intermediate air cooling.

RESULT

This study examined the stress-strain characteristics of a finite element model that incorporated reinforcement bars exhibiting multilinear isotropic hardening. It evaluated the mechanical behavior of 316 alloy samples subjected to different high-temperature exposures and three cooling approaches.

The study indicated that the total maximum strain and user-defined parameters are closely correlated for the virgin material and across the various heating temperatures and cooling modes, as indicated in Figure 5(a-c) under heating temperature of 500°C, 700°C, and 900 °C, with rapid cooling in water. Additionally, it established the maximum equivalent stress values for this heating temperature under rapid cooling in furnace, as depicted in Figure 6 (a-c). The reliability of the finite element model is assessed by comparing it against experimental findings. Table 2 presents a comparison of the ultimate tensile strength (f_u) and proof strength ($f_{0.2p}$) results obtained from both finite element analysis and experimental testing for 316 austenitic stainless steel reinforcing bars subjected to diverse conditions, including the percentage differences between the two approaches. This table concluded that the variation in ultimate tensile strength (f_u) between the experimental and numerical results is less than 2% except for one case which involving slow cooling inside furnace at 500°C (2.5%). Likewise, the difference in 0.2% proof strength ($f_{0.2p}$) is below 2.5%, except for three cases involving rapid water cooling at 500°C (3.2%) and intermediate air cooling at 500°C (3.3%) and 700°C (3.8%). The stress-strain response demonstrates substantial variability depending on the type of cooling methods after heating, as shown in Figure 2. Furthermore, Figure 7(a-c) presents the stress-strain properties of 316 austenitic stainless-steel bars using finite element analysis under heating temperatures of 500°C, 700°C, and 900°C with rapid cooling in water. The result from this figure showed that elevated temperatures result in lower strength and the samples

exhibit greater stress at lower temperatures of 500°C than at elevated temperatures of 900°C.

The simulated data from the finite element analysis correlates well with the data prepared for input into the engineering data at virgin and all temperatures and cooling modes, as presented in Figure 8(a-c) and Figure 9 indicated the cooling method of rapid cooling in water and intermediate air cooling at 500°C showed better mechanical performance than slow cooling inside furnace.

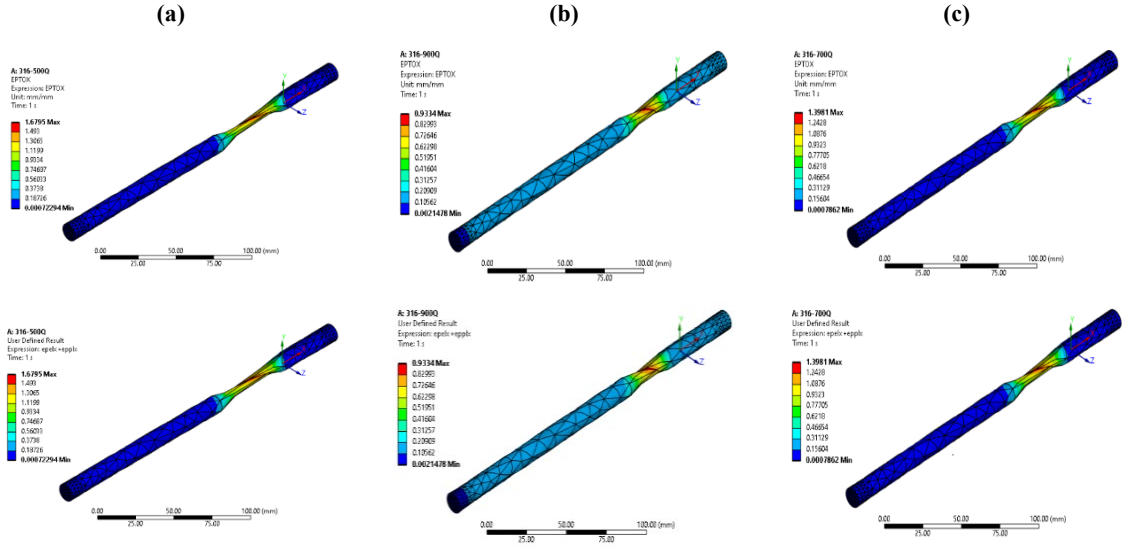

Figure 5. The correlation of total maximum strain(mm/mm) and user defined (the total elastic and total plastic strain) of 316 austenitic stainless steel reinforcing bar at (a) 500°C, (b) 700°C and (c) 900°C following rapid cooling in water.

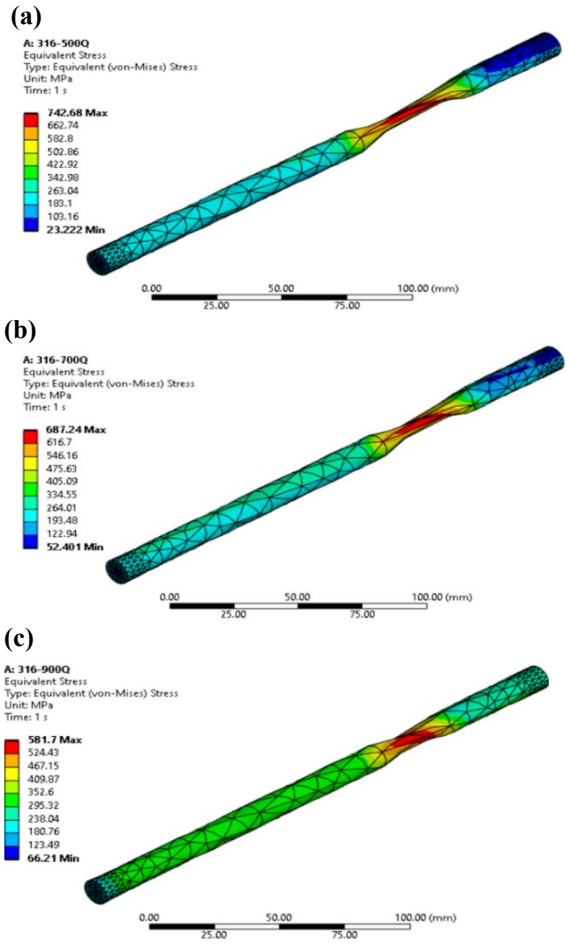

Figure 6. Equivalent stress Maximum (MPa) =742.68, 687.24 and 581.7 for (a) 500 °C, (b) 700 °C and (c) 900 °C respectively following fast cooling in water for 316 austenitic stainless steel reinforcing bar

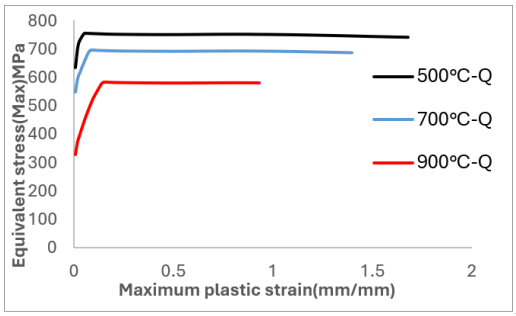

Figure 7. Equivalent stress Maximum (MPa) and maximum plastic strain(mm/mm) response of 316 austenitic stainless steel reinforcing bar for 500°C, 700°C and 900°C following rapid cooling in water.

(a)

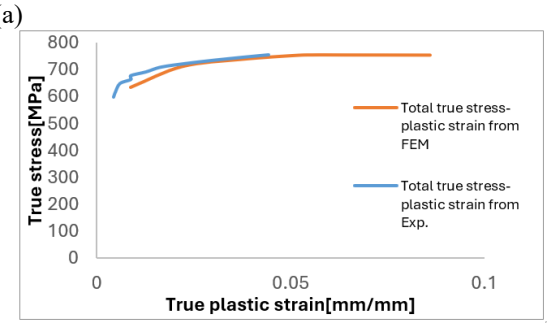

(b)

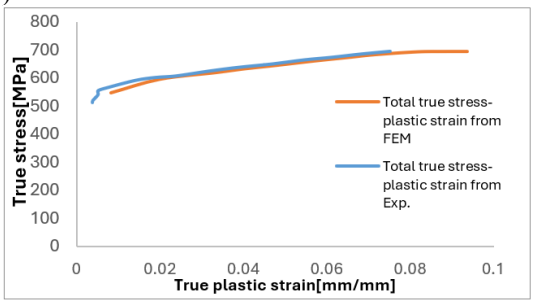

(c)

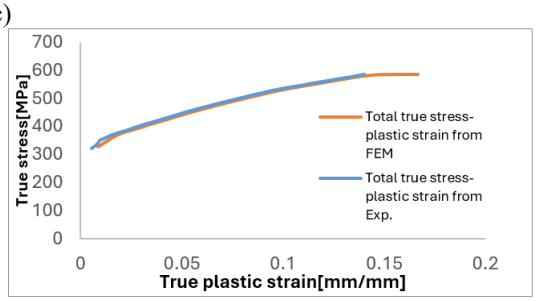

Figure 8. The correlation of total true stress-plastic strain from FE and experimental for 316 austenitic stainless steel reinforcing bar for a) 500 °C, (b) 700 °C and (c) 900 °C following rapid cooling in water.

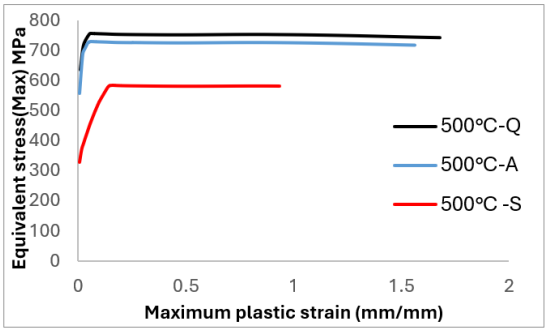

Figure 9. The stress-strain response for 500 °C in three different cooling modes.

The numerical results obtained are consistent with the experimental findings for samples heated to approximately 700°C, indicating minimal changes in strength or ductility across different cooling methods. Based on experimental findings in table 2 which reveals a slight increase of 1-6% in proof strength ($f_{0.2p}$) and an increase of 1-3% in ultimate tensile strength (f_u) compared to the initial values. Upon reverting to normal temperatures following exposure to higher temperatures, the samples either maintained their strength and ductility or showed a decrease (Rehman et al., 2022). Any samples heated to 600°C or higher displayed significant changes in behavior, including a more rounded response, and reduced strength. There was no discernible variance in effectiveness after being subjected to temperatures of 600°C and 900°C; the material's strength performance stayed constant compared to that at lower temperatures and heating caused a decline in the material's strength. Further heating up to 700°C led to an approximately 10-17% decrease in proof strength ($f_{0.2p}$) and a drop of 3-5% in maximum tensile strength (f_u) (Rehman et al., 2022).

In comparison with the original, the proof strength ($f_{0.2p}$) underwent a significant decrease of 49-51% when heated to 900 °C, while the ultimate tensile strength decreased by 19-20% (Rehman et al., 2022). Samples heated to 500 °C then cooled were able to regain their cold working effect; however, exposure to higher temperatures permanently eliminated this effect. A slight alteration in behavior was noted in the samples that underwent different cooling methods. The result of the cooling processes displayed minimal differences in behavior. Bars of Grade 1.4401 that were cooled by air exhibited the least malleability at all temperature conditions, while bars exposed to medium-high temperatures and rapidly quenched with water showed reduced strength compared to other methods (Rehman et al., 2022).

DISCUSSION

There were no notable variances in cooling rates detected between the three investigated cooling conditions. The material response of austenitic grade 1.4401 can be divided into three classifications based on the temperature it experiences. Exposing the material to temperatures up to 500 °C did not result in significant changes in either the proof strength ($f_{0.2p}$) or ultimate tensile strength (f_u) of the samples. The inclusion of molybdenum enhances grade 1.4401's ability to withstand temperatures as high as 500 °C.

The results indicated that samples subjected to a temperature of 700 °C displayed greater strength compared to those not exposed to heat, although the strength was lower than those heated to 500 °C and then cooled. The results showed consistent behavior in samples heated to 700 °C. Samples heated above 700 °C demonstrated higher malleability but lower strength. Complete recrystallization was not accomplished in stainless steel because of inadequate temperature or exposure time, while samples exposed to 900 °C fulfilled the conditions for effective recrystallization. The mechanical properties of austenitic stainless-steel reinforcement were not significantly affected by various cooling methods or rates, as verified by numerical findings.

The results displayed in Table 2, Figure 7 and Figure 8(a-c) demonstrated a strong correlation between experimental data and numerical modeling outcomes.

In Figure 9, the samples subjected to higher elevated temperatures, the quenched samples exhibited greater ductility compared to those cooled more gradually, although the strength levels remained comparable. Under all temperature exposure conditions, the slow-cooled samples exhibited the lowest ductility after the heating and cooling process,

compared to the samples that were either quenched in water or allowed to cool naturally in air.

To sum up, at 500 °C, material properties remain relatively strong, with only minor reductions in strength, at 700 °C, strength decreases, and at 900 °C, the material loses substantial strength, making it unsuitable for high-stress applications. In addition, quenching is the best cooling method for maintaining mechanical strength, while annealing and slow cooling result in softening.

CONCLUSION

The simulations were created to evaluate the effectiveness of advanced numerical models in representing the behavior of cold-worked austenitic stainless-steel reinforcing bar with post-fire mechanical properties. It was observed that accurately depicting the material model and boundary conditions had a considerable impact on the overall response. A cross-comparison could enhance the assessment by providing further broadly applicable insights. The reference values, established through comprehensive testing, showed excellent agreement for all models used. In summary, our investigation yielded these key findings:

The 316 austenitic stainless-steel reinforcing bars retained most of their mechanical characteristics even when subjected to temperatures as high as 700 °C. This study focused on utilizing numerical simulations to evaluate the mechanical response of 316 austenitic stainless-steel reinforcement under different temperature conditions. The stress–strain curves presented in this paper can help the designer in determining the most suitable curves and parameters for various applications. The FE model accurately predicts tensile and proof strength with minor deviations, validating its reliability for further analysis. and this information is essential for applications involving materials subjected to elevated temperatures, including fire safety in structural engineering and high-temperature industrial processes. Eventually, the numerical methods can enhance the precision of experimental results for assessing structural characteristics, which are otherwise uncertain and require extensive efforts using conventional techniques.

ACKNOWLEDGMENT

The authors gratefully acknowledge the Universiti Malaya (UM) for providing the necessary facilities and resources for this research. This research was supported by the Faculty of Engineering Programme under a special funding aid, Bantuan Khas Penyelidikan (BKPFK-2024-15), Universiti Malaya.

REFERENCES

Amanat, K. M. (2025). *Reinforcement for Modern Concrete Structures*. CRC Press.

EN, B. S. (1995). 10088–1. Stainless steels—part 1: list of stainless steels. *British Standards Institution*.

Gudić, S., Vrsalović, L., Matošin, A., Krolo, J., Oguzie, E. E., & Nagode, A. (2023). Corrosion behavior of stainless steel in seawater in the presence of sulfide. *Applied Sciences*, *13*(7), 4366.

Järvenpää, A., Jaskari, M., Kisko, A., & Karjalainen, P. (2020). Processing and properties of reversion-treated austenitic stainless steels. In *Metals* (Vol. 10, Issue 2). MDPI AG. https://doi.org/10.3390/met10020281

Lv, X., Chen, S., Wang, Q., Jiang, H., & Rong, L. (2022). Temperature Dependence of Fracture Behavior and Mechanical Properties of AISI 316 Austenitic Stainless Steel. *Metals*, *12*(9). https://doi.org/10.3390/met12091421

Meza, F. J., Baddoo, N., & Gardner, L. (2024). Derivation of stainless steel material factors for European and US design standards. *Journal of Constructional Steel Research*, *213*, 108383.

Moore, P., & Steels, A. (2010). *Stainless steel grade selection*.

Rehman, F. U., Cashell, K. A., & Anguilano, L. (2022). Experimental Study of the Post-Fire Mechanical and Material Response of Cold-Worked Austenitic Stainless Steel Reinforcing Bar. *Materials*, *15*(4). https://doi.org/10.3390/ma15041564

Shen, Y., & Chacón, R. (2019). Effect of uncertainty in localized imperfection on the ultimate compressive strength of cold-formed stainless steel hollow sections. *Applied Sciences (Switzerland)*, *9*(18). https://doi.org/10.3390/app9183827

Sun, J., Tang, H., Wang, C., Han, Z., & Li, S. (2022). Effects of alloying elements and microstructure on stainless steel corrosion: A review. *Steel Research International*, *93*(5), 2100450.

Version, E. (2014). *Stainless steels-Part 1: List of stainless steels*.

Zapała, R., Kalandyk, B., & Pałka, P. (2022). Effect of temperature on the mechanical properties of X5CrNi18-9 steel. *Metalurgija*, *61*(3–4), 813–815.